Journal of Catalysis 261 (2009) 188–194

Contents lists available at ScienceDirect

Journal of Catalysis

www.elsevier.com/locate/jcat

Atomistic thermodynamics study of the adsorption and the effects of water–gas shift reactants on Cu catalysts under reaction conditions

Nilay İnoğlu [a], John R. Kitchin [a,b,*]

[a] Department of Chemical Engineering, Carnegie Mellon University, Pittsburgh, PA 15213, USA
[b] National Energy Technology Laboratory, Pittsburgh, PA 15236, USA

ARTICLE INFO

Article history:
Received 3 August 2008
Revised 14 November 2008
Accepted 20 November 2008
Available online 20 December 2008

Keywords:
Water–gas shift
Density functional theory calculations
Sulfur
Oxygen
Carbon monoxide
Copper
Thermodynamic analysis

ABSTRACT

Density-functional theory (DFT) calculations were performed to determine the structure and stability of oxygen, carbon monoxide and sulfur adsorption on Cu(111), (100) and (110) surfaces that are in equilibrium with a water–gas shift (WGS) reactive environment of H_2, H_2S, H_2O and CO. An atomistic thermodynamic framework based on DFT was used for describing the phase behaviors of the adsorbates on different Cu facets. Phase diagrams of each possible adsorbate on each surface were constructed as a function of the corresponding chemical potential which showed sulfur poisoning occurs even at ppm levels of H_2S in the environment at low temperatures. Under reaction conditions relevant to WGS at low temperature, CO and S adsorbed surface structures were found to be more stable then the clean catalyst surfaces. At high temperatures and high hydrogen pressures, a poisoned surface can be regenerated back to a clean surface. The shapes of a Cu nanoparticle in the WGS reaction conditions under various sulfur chemical potentials were determined using the Wulff construction. We found that the crystal shape changes significantly from one dominated by (111) and (100) facets at very low sulfur chemical potentials to a shape dominated by (110) facets at higher sulfur chemical potentials, suggesting that reactive site distributions may change under reaction conditions.

1. Introduction

The water–gas shift reaction (WGS) and reverse (RWGS) reaction are widely used in several industrial processes [1,2]. WGS is primarily used to produce high purity hydrogen for ammonia synthesis and RWGS is essential for upgrading CO_2 to CO for use in syngas as a first step in the utilization of CO_2. WGS and its reverse reaction have also an important role in methanol synthesis, where methanol is synthesized from a mixture of CO, CO_2 and H_2 with CO_2 hydrogenation being the major reaction path [3]. Both the methanol synthesis reaction ($CO_2 + 3H_2 \rightarrow CH_3OH + H_2O$) and the water–gas shift reaction ($CO + H_2O \rightleftharpoons H_2 + CO_2$) take place simultaneously.

Cu is the best pure metal for the low temperature water–gas shift reactions [2]. However, Cu catalysts undergo deactivation at temperatures higher than 300 °C due to sintering [4]. The RWGS reaction is much faster than the methanol formation reactions which means methanol yields are usually limited by the WGS equilibrium [5].

In many fossil fuel derived CO_2 feedstocks, there are sulfur (S) impurities which can adsorb on Cu surfaces and block the active sites of the catalyst for the desired reaction and can result in catalyst deactivation [6]. The adsorption of S on surfaces has been widely studied both theoretically and experimentally and this area of study has received great attention due to the fact that S acts as a common poison for most of the metal catalysts and their alloys [6,7]. Even the presence of small amounts of S in the feed streams can cause the deactivation of the catalyst due to the formation of a strong covalent bond between the adsorbate and the surface metal atoms [8–10].

If there is enough S in the reactive environment then inactive copper sulfide phases may form on the catalyst. However, in the RWGS there is a significant hydrogen pressure which could destabilize the adsorbed S by forming H_2S that could desorb from the surface of the Cu catalyst. The extent of destabilization depends on the chemical potentials of the H_2 and H_2S which are determined by the reaction conditions. It is also possible to observe inactive copper oxide phases due to moisture in the reactive environment. However, the presence of H_2 gas could destabilize the adsorbed O by forming H_2O and the extent of destabilization depends this time on the chemical potentials of the H_2 and H_2O that are determined by the reaction conditions. Finally, CO may adsorb competitively blocking sites for S adsorption.

* Corresponding author at: Department of Chemical Engineering, Carnegie Mellon University, Pittsburgh, PA 15213, USA.
E-mail address: jkitchin@andrew.cmu.edu (J.R. Kitchin).

0021-9517/$ – see front matter
doi:10.1016/j.jcat.2008.11.020

Real catalysts are often composed of supported nanoparticles that expose a variety of crystal facets to the reactive environment, each of which may interact differently with the environment. The different interactions with the surfaces may lead to different stabilizing effects on these surfaces, with subsequent changes in the particle morphologies. The low Miller index surfaces, (111), (100) and (110), tend to be the facets with the largest surface areas on particles [11]. This study presents a first principles DFT investigation of CO, O and S adsorption on Cu(111), (100) and (110) facets for coverages between 0.25 and 1.00 ML on a range of different adsorption sites and the impact of that adsorption on the particle shape. Moreover the stability of these different structures are also compared with H and CO_2 adsorbed Cu surfaces.

We present the computational methods used in this work and develop an atomistic thermodynamic framework for evaluating the surface free energy of a Cu surface in the presence of an H_2, H_2S, H_2O and CO environment at different experimental conditions. This paper is organized in the following way. In Section 2 the thermodynamic model for the adsorption of possible adsorbates on Cu facets and the details of the computational methods are given. The adsorption phase diagrams of the adsorbates on each surface are presented in the first part of Section 3. The shapes of a Cu nanoparticle under various chemical potentials, corresponding to various environmental conditions of temperature and pressure, are determined using the Wulff construction and the results are presented in the last part of Section 3. Finally conclusions are provided in Section 4.

2. Theoretical calculations

Our goal is to use DFT calculations to identify thermodynamically relevant adsorption sites and structures in environments that are typical of reaction conditions. It is necessary to develop an atomistic thermodynamic framework [12–17] that relates the DFT results to thermodynamic quantities that are relevant to experimental conditions. With this framework we can consider the stability of different surface structures based on surface free energies that is a function of an appropriate thermodynamic quantity, the Gibbs free energy $G(T,p)$. The basic aim is to determine the composition and atomic structure with the lowest surface free energy for a given temperature and pressure. We first derive the surface free energy framework in the context of Gibbs free energies following the approaches of Reuter and Scheffler [13–15,18] and others [16,17], and then show how to relate the DFT calculations to the required Gibbs free energies.

2.1. Surface energy

The most stable surface composition and geometry is the one that minimizes the surface free energy $\gamma(T,p)$ which is a function of temperature and pressure. We define the surface free energy as

$$\gamma(T,p)=\frac{1}{2A_{\mathrm{surf}}}\Big[G_{\mathrm{slab}}(T,p,N_{\mathrm{Cu}},N_{i^*})-N_{\mathrm{Cu}}\mu_{\mathrm{Cu}}^{\mathrm{bulk}}(T,p)-\sum N_{i^*}\mu_{i^*}(T,p)\Big]. \tag{1}$$

G_{slab} is the Gibbs free energy of a slab with two equivalent (inversion-symmetric) surfaces. N_{Cu} is the number of Cu atoms in the slab and N_{i^*} is the number of possible adsorbates which can be, for example, O*, OH*, CO*, CO_2^*, H*, SH* or S*. $\mu_{\mathrm{Cu}}^{\mathrm{bulk}}$ and μ_{i^*} are the chemical potentials of bulk phase fcc Cu and of any possible adsorbates, respectively. The surface free energy is normalized by the cross sectional area $2A_{\mathrm{surf}}$ of the surface unit cell that defines the slab and accounts for the two equivalent surfaces of the slab. The chemical potential of bulk Cu is equal to the Gibbs free energy of a bulk Cu atom. This approach has previously been used in the investigations of sulfur defects in MoS_2 [16,17].

We now proceed to express the free energies of the solid structures in term of their corresponding DFT energies similar the approach of Reuter and Scheffler [13,14]. Although the framework is written in terms of Gibbs free energies, it is actually *differences* in Gibbs free energies that are most relevant to the surface free energy [14], which we express as $\Delta G=\Delta U-T\Delta S+\Delta(pV)$. For solids, the contribution of $\Delta(pV)$ term is negligibly small because solids are practically incompressible at the conditions relevant to catalysis. The ΔU term is simply described by a difference in total energies at 0 K plus a difference in vibrational energy which is temperature dependent. We calculated the vibrational modes of adsorbed S as 1120 and 2540 cm^{-1} for a coverage of 0.25 ML with S adsorbed at fcc and bridge respectively and vibrational modes of O and CO for a 0.25 ML coverage are obtained as 2044 and 896 cm^{-1} for fcc and atop sites respectively. We determined that the vibrational free energy contribution from the adsorbate [13] to the surface energy stays within 2–6 meV/Å^2 in the temperature range of 10–650 K for all different adsorbates and we neglect these vibrational contributions for the remainder of this manuscript leading $\Delta U=\Delta E$. Reuter and Scheffler reached similar conclusions for oxygen on RuO_2(110) [13]. The second contribution to ΔG is due to configurational entropy. Using a statistical mechanics approach for the configurational entropy contributions [19], we estimate the maximum contribution of configurational entropy to surface energy to be 4 meV/Å^2 and consequently we neglect this contribution. Finally, the approximations that we neglect vibrational free energy and configurational entropy contributions lead us to $\Delta G\approx\Delta E$, which can be directly calculated from density functional theory.

Considering the following equilibrium reactions,

$$\begin{aligned}
&H_2+2^*\rightleftharpoons 2H^*,\\
&H_2S+2^*\rightleftharpoons H^*+SH^*,\\
&SH^*+{}^*\rightleftharpoons S^*+H^*,\\
&H_2O+2^*\rightleftharpoons H^*+OH^*,\\
&OH^*+{}^*\rightleftharpoons O^*+H^*,\\
&CO+{}^*\rightleftharpoons CO^*,\\
&CO_2+{}^*\rightleftharpoons CO_2^*,
\end{aligned} \tag{2}$$

we express the chemical potentials of each possible adsorbate in terms of independent gas phase chemical potentials as

$$\begin{aligned}
&\mu_{H^*}=\frac{1}{2}\mu_{H_2},\\
&\mu_{SH^*}=\mu_{H_2S}-\frac{1}{2}\mu_{H_2},\\
&\mu_{S^*}=\mu_{H_2S}-\mu_{H_2},\\
&\mu_{OH^*}=\mu_{H_2O}-\frac{1}{2}\mu_{H_2},\\
&\mu_{O^*}=\mu_{H_2O}-\mu_{H_2},\\
&\mu_{CO^*}=\mu_{CO},\\
&\mu_{CO_2^*}=\mu_{CO_2},
\end{aligned} \tag{3}$$

where μ_{H_2}, μ_{H_2S}, μ_{H_2O}, μ_{CO} and μ_{CO_2} are the chemical potentials of gas phase H_2, H_2S, H_2O, CO and CO_2 respectively.

The chemical potential of an ideal gas $\mu_{\mathrm{gas}}(T,p)$ can be expressed as

$$\mu_{\mathrm{gas}}(T,p)=\mu_{\mathrm{gas}}^0(T,p^0)+kT\ln\left(\frac{p}{p^0}\right), \tag{4}$$

where the last term is the contribution due to the deviation from the reference pressure p^0 and accounts for the pV dependence of the Gibbs free energy of the gas-phase environment. $\mu^0_{\text{gas}}(T, p^0)$ can be described in terms of the internal energy of the system at 0 K, the change in Gibbs free energy due to a change in temperature from 0 K. Assuming H_2S, H_2O, H_2, CO_2 and CO to behave like ideal gases, the chemical potential of these gases can be expressed as

$$\mu_{\text{gas}}(T, p) = E_{\text{gas}}(0\ \text{K}) + \Delta G_{\text{gas}}(\Delta T, p^0) + kT \ln\left(\frac{p_{\text{gas}}}{p^0}\right). \tag{5}$$

Using the relation $G = H - TS$ and choosing $p^0 = 1$ atm, the experimental data for the enthalpy and entropy can be found in standard thermodynamic tables [20]. For instance for the S chemical potential, this leads μ_{S^*} to be written as

$$\begin{aligned}\mu_{S^*} = {} & \left[E_{H_2S}(0\ \text{K}) - E_{H_2}(0\ \text{K})\right] \\ & + \left[\Delta H(\Delta T, p^0, H_2S) - \Delta H(\Delta T, p^0, H_2)\right] \\ & - T\left[\Delta S(\Delta T, p^0, H_2S) - \Delta S(\Delta T, p^0, H_2)\right] \\ & + kT \ln\left(\frac{p_{H_2S}}{p_{H_2}}\right).\end{aligned} \tag{6}$$

Similar expressions for μ_{S^*} were derived in the studies of the stability of MoS_2 [17] and Pd [21] in H_2/H_2S environments.

There are practical limits on the range of possible adsorbate chemical potentials that correspond to experimentally relevant conditions. For S adsorption, if the S chemical potential becomes equal to or greater than that of bulk S (S-rich conditions) then S will begin to condense on the surface and form the bulk S phase (in addition to possibly forming bulk Cu sulfides) on the Cu surface leading to a total deactivation of the catalyst. There is no lower limit for the S chemical potential; a chemical potential of $-\infty$ corresponds to a gas-phase environment with no sulfur in it. Using the α phase of S for E_S^{Bulk} and shifting the limits to have the S-rich chemical potential at zero, the range for the S chemical potential is written as

$$-\infty \leqslant \mu_{S^*} - E_S^{\text{Bulk}} \leqslant 0, \tag{7}$$

where $\mu_{S^*} - E_S^{\text{Bulk}}$ is defined to be $\Delta\mu_S$.

Similarly, the range for O and CO chemicals potentials are expressed as

$$\begin{aligned}-\infty \leqslant \mu_{O^*} - \frac{1}{2}E_{O_2} \leqslant 0, \\ -\infty \leqslant \mu_{CO^*} - E_{CO} \leqslant 0,\end{aligned} \tag{8}$$

where $\mu_{O^*} - \frac{1}{2}E_{O_2}$ and $\mu_{CO^*} - E_{CO}$ are defined to be $\Delta\mu_O$ and $\Delta\mu_{CO}$ respectively.

2.2. Adsorption energies and surface free energies

The adsorption energy is defined (in the approximation where $\Delta G \cong \Delta E$ for solids) as

$$\Delta H_{\text{ads}} = E_{\text{slab}+i} - E_{\text{slab}} - \sum N_{i^*}\mu_{i^*}, \tag{9}$$

where $E_{\text{slab}+i}$ is the total energy of the Cu slab with possible adsorbates while E_{slab} is the energy of the clean slab. Substituting in the expressions for the chemical potentials of the possible adsorbed species, the adsorption energies can be written as

$$\begin{aligned}\Delta H_{\text{ads}} = {} & E_{\text{slab}+i} - E_{\text{slab}} - \frac{1}{2}N_{H^*}E_{H_2} - N_{SH^*}\left(E_{H_2S} - \frac{1}{2}E_{H_2}\right) \\ & - N_{S^*}(E_{H_2S} - E_{H_2}) - N_{OH^*}\left(E_{H_2O} - \frac{1}{2}E_{H_2}\right) \\ & - N_{O^*}(E_{H_2O} - E_{H_2}) - N_{CO^*}(E_{CO}) - N_{CO_2^*}(E_{CO_2}) \\ & - \frac{1}{2}N_{H^*}\delta\mu_{H_2} - N_{SH^*}\left(\delta\mu_{H_2S} - \frac{1}{2}\delta\mu_{H_2}\right) \\ & - N_{S^*}(\delta\mu_{H_2S} - \delta\mu_{H_2}) - N_{OH^*}\left(\delta\mu_{H_2O} - \frac{1}{2}\delta\mu_{H_2}\right) \\ & - N_{OH^*}(\delta\mu_{H_2O} - \delta\mu_{H_2}) - N_{CO^*}(\delta\mu_{CO}) \\ & - N_{CO_2^*}(\delta\mu_{CO_2})\end{aligned} \tag{10}$$

with $\delta\mu_i = \Delta G_i(\Delta T, p^0) + kT \ln(p_i/p^0)$.

Using the definition of the adsorption energy, the surface energy of a considered structure can be expressed through Eq. (1) as follows,

$$\gamma(T, p) = \gamma_{\text{clean}} + \frac{\Delta H_{\text{ads}}(0\ \text{K})}{A_{\text{surf}}} - \frac{\sum N_{i^*}\delta\mu_{i^*}(T, p)}{A_{\text{surf}}}, \tag{11}$$

with γ_{clean} being the clean surface energy and $\Delta H_{\text{ads}}(0\ \text{K})$ being the adsorption energy calculated at absolute zero.

In the limiting case of a single type of adsorbate on the Cu surface at 0 K, Eq. (10) is written as follows for individual adsorption of S, O and CO respectively,

$$\begin{aligned}\Delta H^{S}_{\text{ads}}(0\ \text{K}) &= E_{\text{slab}+S} - E_{\text{slab}} - N_{S^*}(E_{H_2S} - E_{H_2}), \\ \Delta H^{O}_{\text{ads}}(0\ \text{K}) &= E_{\text{slab}+O} - E_{\text{slab}} - N_{O^*}(E_{H_2O} - E_{H_2}), \\ \Delta H^{CO}_{\text{ads}}(0\ \text{K}) &= E_{\text{slab}+CO} - E_{\text{slab}} - N_{CO^*}(E_{CO}).\end{aligned} \tag{12}$$

The surface energy can then be expressed in the following intuitive form:

$$\gamma(T, p) = \gamma_{\text{clean}} + \frac{\Delta H^{i}_{\text{ads}}(0\ \text{K})}{A_{\text{surf}}} - \frac{N_{i^*}\Delta\mu_{i^*}(T, p)}{A_{\text{surf}}} \tag{13}$$

with i being S, O or CO. The surface free energy is seen to be composed of a contribution from the clean surface energy, a contribution due to adsorption, and a contribution from the environmental conditions. Each of these terms can be calculated independently. The clean surface free energy is the only result that needs to be calculated with inversion symmetric slabs. The adsorption energies can be calculated from slabs with adsorption on a single side, and the last term depends only on the reactive environment conditions.

2.3. Total energy calculations and convergence

S adsorption energies at coverages of 0.25, 0.50, 0.75 and 1.00 ML in fcc, hcp, fourfold hollow, bridge and atop sites on the Cu(111), (100) and (110) surfaces were determined using DFT calculations where a total of 43 different structures were considered. O adsorption energies were calculated at different coverages ranging between 0.25 and 1.00 ML at fcc adsorption site which was found to be the most stable adsorption site in previous studies [22,23]. Similarly, CO adsorption energies were determined at the atop site [24,25] at coverages between 0.25 and 1.00 ML. We utilized the DACAPO code for all the DFT calculations in this work [26]. The electronic structures were obtained using the generalized gradient approximation (GGA) for the exchange functional correlation due to Perdew and Wang (PW91) [27]. The core electrons were described by Vanderbilt ultrasoft pseudopotentials [28–30] and the one electron valence eigenstates were expanded in a plane wave basis set with a cutoff energy of 340 eV.

The lattice constant of bulk Cu was calculated as 3.64 Å using the Murnaghan equation of state [31] which is in good agreement with the established experimental value of 3.61 Å [32,33]. This value also agrees with previously reported results for the PW91 exchange-correlation functional [34].

The Cu(111) surface was modeled using a 5-layer slab with adsorbate coverage on one side while the Cu(100) and Cu(110) surfaces were modeled with 6-layer and 8-layer slabs respectively, preserving the thickness of each slab to be approximately 9 Å.

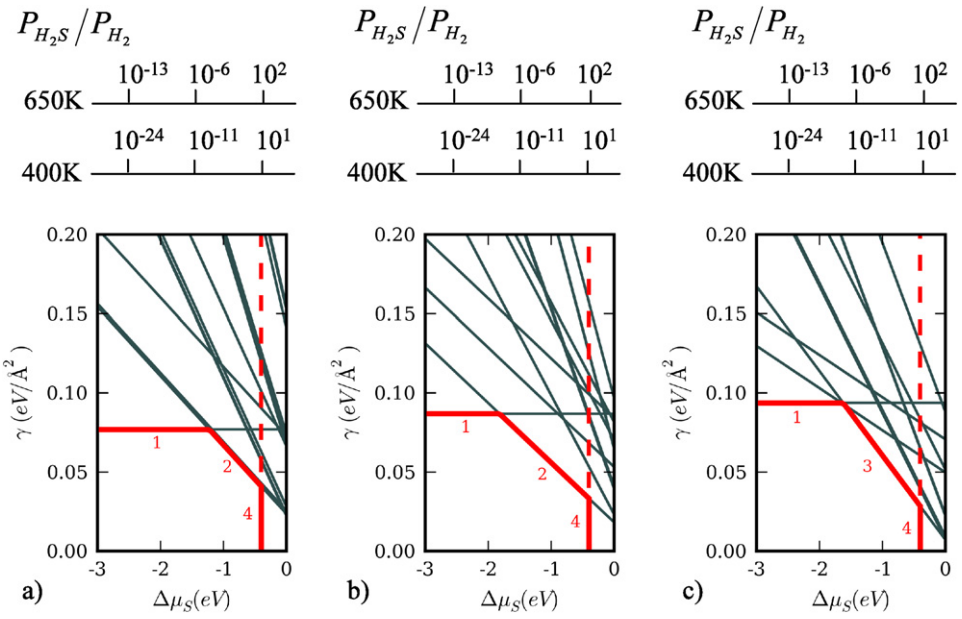

Fig. 1. Calculated surface energies as a function of the change in S chemical potential for (a) Cu(111), (b) Cu(100) and (c) Cu(110). The bold red line indicates the most stable surface energy at each chemical potential. The inset numbers show the structure that corresponds to the most stable surfaces: (1) clean surface, (2) surface with adsorbate of 0.25 ML coverage, (3) surface with adsorbate of 0.50 ML coverage, (4) formation of bulk Cu sulfide.

A dipole correction scheme was tested and found to be unnecessary in these calculations. The vacuum region between the repeated slabs was 10 Å. Brillouin-zone integrations were performed using a $12 \times 12 \times 1$ Monkhorst-Pack grid for the 1×1 surface unit cell and $6 \times 6 \times 1$ for the 2×2 surface cell. For all of our calculations, the adsorbed atoms and the upper two layers were relaxed until the forces were less than 0.05 eV/Å, whereas the other layers were frozen at the bulk Cu coordinates. These parameters were chosen to ensure that the calculated adsorption energies were converged with an estimated numerical uncertainty of less than 0.05 eV/adsorbate. These numerical uncertainties in the adsorption energies lead to a typical uncertainty of ± 4 meV/Å^2 in $\gamma(T, p)$ which is small enough not to significantly affect the conclusions drawn in this work. The energies of the gas phase H_2S, H_2O, CO and H_2 molecules were calculated in a $10 \times 10 \times 10$ Å^3 box.

3. Results and discussion

Sulfur forms strong bonds to all the Cu surfaces at low coverages. This shows that Cu is susceptible to S poisoning which is consistent with an experimental study of Campbell and Koel [35] who reported that Cu-based catalysts poison even at ppm levels of H_2S. We observed that S adsorbs preferentially on the most highly coordinated sites for the three surfaces of Cu examined in this work. This is consistent with literature reports of S adsorption on Cu and other metal surfaces [6,7].

For most of the highly coordinated adsorption sites, we observed an adsorbate-induced surface electronic structure modification that broadened the surface *d*-band while maintaining the same number of filled *d*-states. The surface *d*-band broadening with increasing coverage corresponded to a decrease in the *d*-band center and to weakening of the S adsorption energies. This effect was not observed for the lowest coordinated adsorption (atop) sites. The details of S adsorption on Cu surfaces and changes in electronic structures will be given in a future manuscript.

Atomic or molecular oxygen adsorption on Cu systems is reported to be quite favorable with highly negative adsorption energies of -4.5 eV/O atom at the fcc adsorption site [22]. When moisture in the environment is considered as the source of O atoms, the O adsorption energies are -0.3 eV/O. The adsorption of O from H_2O is less exothermic than from dissociation of O_2 due to the stability of the H_2O molecule compared to O_2 or gas-phase O atom adsorption. The calculated CO adsorption energy of -0.65 eV/CO at the atop site at 0.25 ML over Cu(111) is reasonably similar to reported experimental value of -0.5 eV/CO [25]. All of the adsorption energies in this work are presented here through their role in the surface free energy equation (13) in the next section.

Relative stability and Cu catalyst morphology

We calculated the surface energies for each adsorbate in each adsorption site and coverage and determined the relative stabilities of these configurations under different environmental conditions according to Eq. (13). We first consider only the environments that would lead to individual adsorbates, and later consider adsorption in multicomponent environments relevant to WGS conditions. For Cu surfaces in contact with H_2S and H_2, the calculated surface energies of each of the considered adsorption structures (all sites and coverages) are shown in Fig. 1 for each different facet. In these figures, the S chemical potential at which the bulk CuS phase starts to form is also considered. The heat of formation is

$$\Delta H^f_{\mathrm{CuS}} = E^{\mathrm{Bulk}}_{\mathrm{CuS}} - E^{\mathrm{Bulk}}_{\mathrm{Cu}} - \mu_{S^*}, \tag{14}$$

where μ_{S^*} is the S chemical potential; while $E^{\mathrm{Bulk}}_{\mathrm{CuS}}$ and $E^{\mathrm{Bulk}}_{\mathrm{Cu}}$ are the energies of bulk CuS and Cu respectively. The calculated value of $\Delta H^f_{\mathrm{CuS}}$ is -0.40 eV, and this is plotted in the surface energy graphs in Fig. 1 as the vertical dashed line in red. At chemical potentials higher than -0.40 eV, the formation of bulk CuS is thermodynamically favorable. Other bulk sulfide stoichiometries could also be considered, but they were not in this work. The S chemical potential can be expressed in terms of temperature and pressure through Eq. (6). In each figure we present a range of partial pressure ratio values that correspond to two fixed temperatures of 400 K and 650 K.

At low S chemical potentials (less than -1.25 eV), the clean surfaces are most stable in each case. On Cu(111), the most favorable adsorbate structure becomes S adsorbed at the fcc site at 0.25 ML

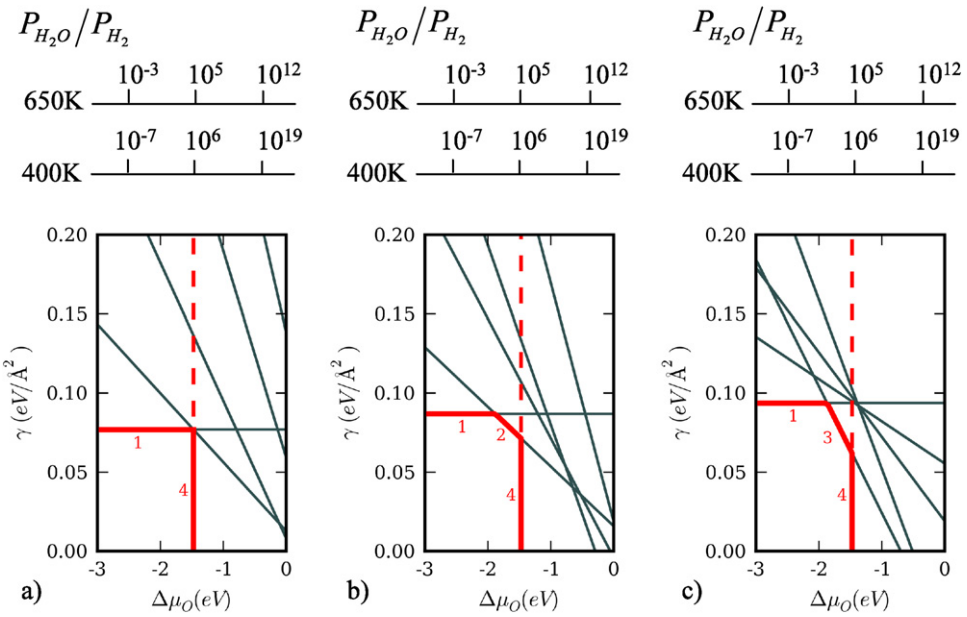

Fig. 2. Calculated surface energies as a function of the change in O chemical potential for (a) Cu(111), (b) Cu(100) and (c) Cu(110). The bold red line indicates the most stable surface energy at each chemical potential. The inset numbers corresponds to: (1) clean surface, (2) surface with adsorbate of 0.25 ML coverage, (3) surface with 0.75 ML coverage, (4) formation of bulk Cu oxide.

coverage at a S chemical potential of −1.25 eV to −0.40 eV, after which the formation of bulk CuS is thermodynamically favorable, although the bulk sulfide formation could be kinetically limited. On Cu(100), S adsorption at the fourfold hollow site at a coverage of 0.25 ML is the most stable surface between −1.85 eV to −0.40 eV. Thereafter, bulk CuS is the most stable structure. On Cu(110), S adsorption on fourfold sites with a coverage of 0.50 ML becomes favorable at −1.65 eV. When the S chemical potential reaches −0.40 eV, again bulk CuS formation is observed.

Fig. 1 shows that very small H_2S/H_2 ratios are required to avoid S adsorption on Cu surfaces. For instance, on Cu(111) in contact with 1 ppm H_2S at 400 K a hydrogen pressure of roughly 10^3 atm is required to avoid S poisoning which supports the idea that Cu is very susceptible to S poisoning. We have also checked the stability of H adsorbed Cu(111) systems under a fixed H_2 pressure of 25 atm (typical of the operating pressure in WGS reactions) and 1 ppm of H_2S (corresponding to a S chemical potential of 4×10^{-8}). We found out that for 400 K, the surface energies of S poisoned structures are lower than the surface energy of H-terminated surfaces or clean surfaces. This shows that at low temperatures, S poisoning is unavoidable. The situation is different with the same pressures at 650 K. Under these conditions the clean surface was the thermodynamically most stable structure. Thus, high temperatures and high H_2 pressures can be used to regenerate S-poisoned slab back to a clean surface, although if the temperatures are too high than sintering and loss of surface area may be a concern.

The calculated surface energies of O and CO adsorbed Cu systems are shown in Figs. 2 and 3 for each different facet as a function of O and CO chemical potentials respectively. In Fig. 2, the O chemical potential at which the formation of bulk CuO phase becomes thermodynamically stable is calculated similar to Eq. (14) and this is plotted in the surface energy graphs as the vertical dashed line in red. In each figure we present the chemical potentials in terms of gas-phase pressures at the same fixed temperatures of 400 K and 650 K. Similar to the S poisoned structures, at low O chemical potentials the clean surface is the most stable surface structure; as μ_O increases, oxygen adsorption at 0.25 ML becomes stable in a very narrow chemical potential window on the Cu(111) and in a broader window on the (100) surface, which is then followed by the formation of bulk CuO (Fig. 2). However, for the Cu(110) surface a partially oxidized surface with 0.75 ML of oxygen is more stable than lower coverages of adsorbed oxygen atoms.

For the CO adsorbed Cu systems, a coverage of 0.25 ML on the atop sites is stable first, followed by 0.5 ML on the atop sites (Fig. 3). Higher coverages are not predicted to be stable at the temperatures considered in this work. We have also compared the stability of CO_2 adsorbed Cu structures under a fixed CO_2 pressure of 5.5 atm and we concluded that at both temperature values, CO_2 adsorption is thermodynamically less favorable than the S-poisoned slab at 400 K and than the clean surface at 650 K. Similarly, the stability check of H and CO_2 adsorbed Cu systems showed that O adsorbed surface structures are more stable than these at 400 K, although oxygen covered surfaces could be regenerated to clean Cu surfaces at 650 K.

There are many other adsorption configurations, including mixed adsorbate phases, which could potentially have lower surface energies than the ones considered in this work. It is infeasible to consider them all with the density functional theory approach used in this work. Nevertheless, even from our limited set of configurations we conclude that Cu surfaces could be covered by S, O or CO adsorbed structures depending on the environmental conditions.

Under WGS reaction conditions there are substantial pressures of H_2, H_2O, CO_2, and CO with trace levels of H_2S. We now consider which adsorbates are likely to exist on the surface under these conditions. In typical WGS reaction conditions with a total pressure of 50 atm, we choose the gas phase composition as 10% CO, 51% H_2, 11% CO_2 and 28% H_2O similar to the composition in the study of Gokhale and co-workers [36]. We also assume an H_2S concentration of 1 ppm, giving a partial pressure ratio of H_2S/H_2 of 10^{-8}. Under these conditions the Cu surfaces are not clean, but partially covered by CO due to its stronger adsorption energy than oxygen adsorbates from water. It is still possible some S could be adsorbed on the surface under these conditions, although mixed phases were not considered. At higher concentrations of H_2S in the reactive environment, S-terminated surfaces eventually become more stable than any other adsorbate covered surface (as shown in Fig. 4). Most significantly, the surface energies

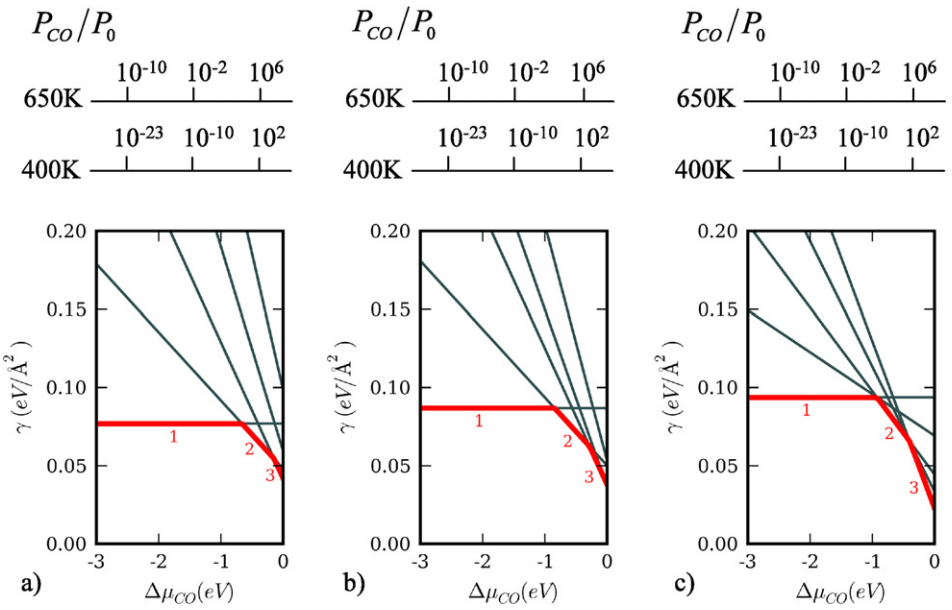

Fig. 3. Calculated surface energies as a function of the change in CO chemical potential for (a) Cu(111), (b) Cu(100) and (c) Cu(110). The bold red line indicates the most stable surface energy at each chemical potential. The inset numbers corresponds to: (1) clean surface, (2) surface with adsorbate of 0.25 ML coverage, (3) surface with adsorbate of 0.50 ML coverage.

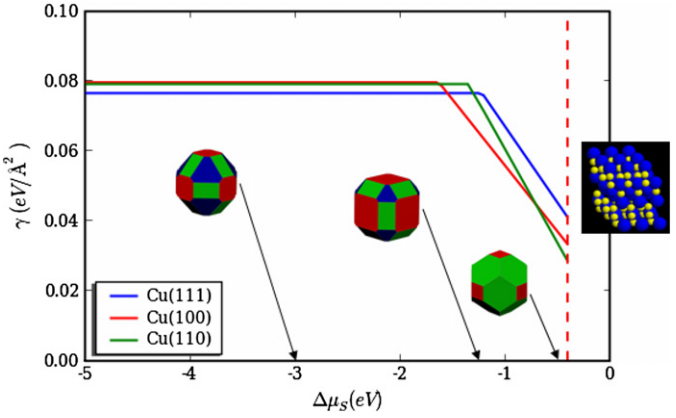

Fig. 4. Surface energies of the most favorable structures for all different facets and the corresponding morphology predicted by the Wulff construction at different sulfur chemical potentials. The flat lines of each different facet correspond to CO terminated structures of the facets.

of each facet change differently with the sulfur chemical potential.

A real catalyst particle will have various amounts of each of the three surfaces considered in this work. Other higher Miller index surfaces could also exist, but we limit our discussion here to the most common low Miller index surfaces because they dominate the surface areas of nanoparticles [11]. The equilibrium shape (i.e., the distribution of reactive sites from each crystal surface) of the catalyst particle is determined by minimizing the total surface free energy (neglecting edge and corner effects), subject to the constraint of a constant volume particle using the Wulff construction [37]. Since the surface energies of each facet are a function of the sulfur chemical potential, then the equilibrium particle shape should also be a function of the sulfur chemical potential. We took the most stable surfaces under WGS reaction conditions and compared them to the most stable S-terminated surfaces as a function of sulfur chemical potential to determine the lowest surface energy structures on each facet for varying levels of H_2S in the reactive environment. The results are summarized in Fig. 4.

The equilibrium crystal shape can be determined from a Wulff construction under different S chemical potentials that corresponds to different experimental conditions of temperatures and pressures [37]. We constructed 3D crystal structures at different S chemical potentials from the surface energies in Fig. 4 using the program WINXMORPH [38,39], similar to the study of Soon et al. where the morphology of Cu particles were determined in nitrogen atmospheres [40]. We found out that the crystal shape changes significantly from one dominated by (111) and (100) facets at very low S chemical potentials to a shape dominated by (110) facets at high chemical potentials. These results show that the distribution and number of active sites on catalyst particles may have a significant dependence on the reactive environment they are in. Although we do not consider supported particles in this work, the principles determining the particle shape are the same. The support is like another reactive environment that modifies the surface (or interfacial) energy of the particle, and consequently the particle shape. Reactive environment-induced shape changes on Cu catalysts have previously been experimentally observed [37]. In that work a change from a reducing atmosphere to an oxidizing atmosphere resulted in shape changes visible to a TEM. This work suggests that reactive environment-induced shape changes due to adsorption may be a general phenomena. Our work is one approach to accounting for particle shape changes, and the consequential change in the number of active sites that occur as a result of the reactive environment.

4. Conclusions

In this study we performed density functional theory calculations to investigate the interactions between adsorbates and low Miller index facets of Cu in the presence of a reactive environment containing H_2, H_2S, H_2O, CO and CO_2. We utilized a first principles atomistic thermodynamics approach to evaluate the stability of different adsorbate structures on Cu surfaces in contact with a reactive environment through the surface free energy of the structures. Adsorbate phase diagrams on each surface were constructed which showed S poisoning occurs even at ppm levels of H_2S in the environment at low temperatures. The effect of hydrogen gas in destabilizing the adsorbed S was found to be effective

at elevated temperatures. We determined that under experimental reactive environment conditions, CO and S adsorbed surface structures have the lowest surface energies and they control the Cu crystal morphologies. The shape of a Cu particle under different chemical potentials corresponding to different experimental conditions of temperatures and pressures was determined based on the Wullf construction. We found the shape changed from one dominated by (111) and (100) facets at very low chemical potentials to a shape dominated by (110) facets at high chemical potentials, indicating that the reactive site distribution may change under reaction conditions.

References

[1] G.C. Wang, L. Jiang, X.Y. Pang, Z.S. Cai, Y.M. Pan, X.Z. Zhao, Y. Morikawa, J. Nakamura, Surf. Sci. 543 (2003) 118.
[2] N. Schumacher, A. Boisen, S. Dahl, S. Kandoi, L.C. Grabow, J.A. Dumesic, M. Mavrikakis, I. Chorkendorff, J. Catal. 229 (2005) 265.
[3] J. Yoshihara, C.T. Campbell, J. Catal. 161 (1996) 776.
[4] M. Twigg, M. Spencer, Appl. Catal. 212 (2001) 161.
[5] M. Maack, H. Friis-Jensen, S. Sckerl, J.H. Larsen, I. Chorkendorff, Top. Catal. 22 (2003) 160.
[6] D.R. Alfonso, A.V. Cugini, D.S. Sholl, Surf. Sci. 546 (2003) 12.
[7] M. May, S. Gonzalez, F. Illas, Surf. Sci. 602 (2008) 906.
[8] J.A. Rodriguez, S. Chatuvedi, T. Jirsak, Chem. Phys. Lett. 296 (1998) 421.
[9] P.A. Gravil, H. Toulhoat, Surf. Sci. 430 (1999) 176.
[10] F.J. Feibelman, D.R. Hamann, Surf. Sci. 149 (1985) 48.
[11] R.I. Masel, Principles of Adsorption and Reaction on Solid Surfaces, John Wiley & Sons, New York, 1996.
[12] J.R. Kitchin, K. Reuter, M. Scheffler, Phys. Rev. B 77 (2008) 075347.
[13] K. Reuter, M. Scheffler, Phys. Rev. B 65 (2001) 035406.
[14] K. Reuter, M. Scheffler, Phys. Rev. B 68 (2003) 045407.
[15] K. Reuter, M. Scheffler, Phys. Rev. B 90 (2003) 046103.
[16] P. Raybaud, J. Hafner, G. Kresse, S. Kasztelan, H. Toulhoat, J. Catal. 189 (2000) 129–146.
[17] M.V. Bollinger, K.W. Jacobsen, J.K. Nørskov, Phys. Rev. B 67 (2003) 085410.
[18] J. Rogal, K. Reuter, M. Scheffler, Phys. Rev. B 69 (2004) 075421.
[19] D.A. McQuarrie, Statistical Mechanics, University Science Books, Sausalito, CA, 2000.
[20] D.R. Stull, H. Prophet, JANAF Thermochemical Tables, U.S. National Bureau of Standards, Washington, DC, 1971.
[21] D.R. Alfonso, Surf. Sci. 601 (2007) 4899.
[22] A. Soon, M. Todorova, B. Delley, C. Stampfl, Phys. Rev. B 73 (2006) 165424.
[23] Y. Li, J.M. Hu, Y.F. Zhang, J.Q. Li, Appl. Surf. Sci. 252 (2006) 5636.
[24] C.D. Zeinalipour-Yazdi, A.L. Cooksy, A.M. Efstathiou, Surf. Sci. 602 (2008) 1858.
[25] F. Abild-Pedersen, M.P. Andersson, Surf. Sci. 601 (2007) 1747.
[26] http://www.fysik.dtu.dk/CAMPOS.
[27] J.P. Perdew, K. Burke, M. Ernzerhof, Phys. Rev. B 77 (1996) 3865.
[28] D. Vanderbilt, Phys. Rev. B 41 (1990) 7892.
[29] K. Laasonen, A. Pasquarello, R. Car, C. Lee, D. Vanderbilt, Phys. Rev. B 47 (1993) 10142.
[30] http://www.physics.rutgers.edu/.
[31] F.D. Murnaghan, Proc. Natl. Acad. Sci. 50 (1994) 697.
[32] http://www.webelements.com.
[33] C. Kittel, Introduction to Solid State Physics, Wiley, New York, 1996.
[34] Z. Crljen, P. Lazic, D. Sokcevic, R. Brako, Phys. Rev. B 68 (2003) 195411.
[35] C.T. Campbell, B.E. Koel, Surf. Sci. 183 (1987) 100.
[36] A.A. Gokhale, J.A. Dumesic, M. Mavrikakis, J. Am. Chem. Soc. 130 (2008) 1402.
[37] P.L. Hansen, J.B. Wagner, S. Helveg, J.R. Rostrup-Nielsen, B.S. Clausen, H. Topsøe, Science 295 (2002) 2053.
[38] W.J. Kaminsky, Appl. Crystallogr. 38 (2005) 566.
[39] W.J. Kaminsky, Appl. Crystallogr. 40 (2007) 382.
[40] A. Soon, L. Wong, B. Delley, C. Stampfl, Phys. Rev. B 77 (2008) 125423.